2013 IEEE/RSJ International Conference on
Intelligent Robots and Systems (IROS)
November 3-7, 2013. Tokyo, Japan

# Nanorobotic *in situ* Characterization of Nanowire Memristors and "Memsensing"

Zheng Fan, *Student Member, IEEE*, Xudong Fan, Alex Li, and Lixin Dong, *Senior Member, IEEE*

***Abstract* — We report the nanorobotic in situ forming and characterization of memristors based on individual copper oxide nanowires (CuO NWs) and their potential applications as nanosensors with memory (memristic sensors or "memsensors"). A series of in situ techniques for the experimental investigations of memristors are developed including nanorobotic manipulation, electro-beam-based forming, and electron energy loss spectroscopy (EELS) enabled correlation of transport properties and carrier distribution. All experimental investigations are performed inside a transmission electron microscope (TEM). The initial CuO NW memristors are formed by localized electron-beam irradiation to generate oxygen vacancies as dopants. Current-voltage properties show distinctive hysteresis characteristics of memristors. The mechanism of such memristic behaviors is explained with an oxygen vacancy migration model. The presence and migration of the oxygen vacancies is identified with EELS. Investigations also reveal that the memristic behavior can be influenced by the deformation of the nanowire, showing that the nanowire memristor can serve as a deformation/force memorable sensor. The CuO NW-based memristors will enrich the binary transition oxide family but hold a simpler and more compact design than the conventional thin-film version. With these advantages, the CuO NW-based memristors will not only facilitate their applications in nanoelectronics but play a unique role in micro-/nano-electromechanical systems (MEMS/NEMS) as well.**

***Index Terms* — in situ nanotechnology, nanorobotic manipulation, memristor, memsensor**

## I. Introduction

The first experimental demonstration of a memristor (short for "memory resistor") in 2008 has stimulated fast expanding interests in nanoelectronics due to its unique circuit properties such as current-voltage hysteresis and time-dependent resistance [1]. Metal oxides, such as $TiO_2$, $Nb_2O_5$, NiO and ZnO are the most common raw materials for the fabrication of memristive devices due to their resistive transition behaviors [2-3]. The conventional setup of these materials to be used as memristors takes a thin-film design. These thin-film structured memristors have great advantages such as low-energy electroforming and high switching speed [2, 4]. Therefore, it is the natural choice for the next generation non-volatile random-access memory (NVRAM). On the other hand, the interest in memristors based on 1D materials such as nanowires are stimulated by their simpler and more compact design, which will also lead to a higher integration density [5-7].

As a new fundamental element for electronics, a memristor may also open new possibilities in the development of nanosensors, providing an additional transduction mechanism to piezoresistivity/piezoelectricity, magnetoresistivity, and capacitance [7]. For instance, because a memristor can memorize the voltage that applied on it, a memristor-based sensor can have the historical information of force/deformation/chemical doping recorded, resulting in a sensor of the ability of memory, or a "memsensor". While a variety of new possibilities of "memsensors" are pending for discovery, we tackle the feasibility in this report.

Previous experimental investigations are typically *ex situ*, i.e., the transport properties have been investigated before and after the switching occurred. This is partly due to the setup of the thin-film based memristor where active metal oxide regions are buried under the metal electrode contact, which prevented *in situ* investigation. Furthermore, the thin-film based two-dimensional memristor has limited the flexibility to be extended to other forms of devices such as transducers. To understand the memristic switching mechanism, *in situ* investigations on conducting filament growth/dissolution have been reported by two groups recently [8-9]. Based on these advancements, here we report electron-beam (e-beam) based *in situ* forming of a nanowire memristor and the correlation of its structural changes during the forming and switching behaviors. All investigations have been performed inside a transmission electron microscope (TEM) using electron beam irradiation, nanomanipulation and electron energy loss spectroscopy (EELS) for its forming, characterization and applications. In the following, we will first describe the implementation and characterization of this nanowire-based memristor with nanorobotic manipulation, and then address its mechanism as well as its applications.

## II. Experimental Setup

Z. Fan and L. X. Dong are with the Department of Electrical and Computer Engineering, Michigan State University, East Lansing, MI 48824-1226, USA (phone: 517-353-3918; fax: 517-353-1980; e-mail: ldong@egr.msu.edu).

X. D. Fan is with the Center of Advance Microscopy, Michigan State University, East Lansing, MI 48824-1226, USA.

A. Li is with the Air Force Institute of Technology, Wright-Patterson AFB, OH 45433-7765, USA.

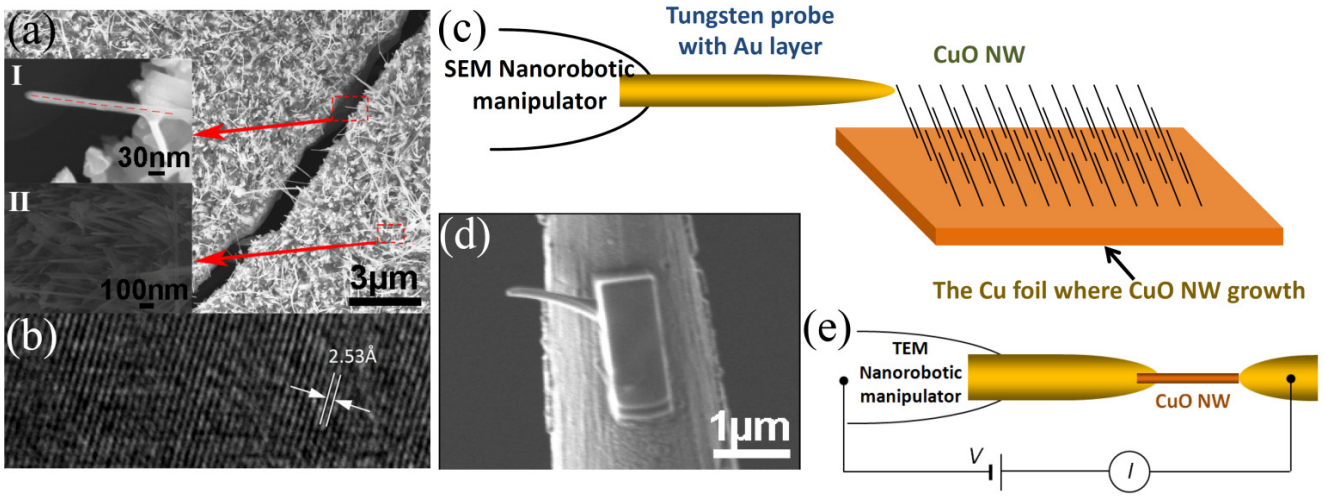


Fig.1 Synthesis and manipulation of CuO NWs (a) Non-flaking nanowire arrays were grown on the surface of a copper substrate after 2-hour incubation in a box oven at 500℃. Inset I shows an enlarged SEM image of a single nanowire. Inset II shows that as-fabricated nanowires are distributed in the substrate at a high density of about 4~6 wires per 100 square nanometers. (b) HRTEM image indicates an inter-planar spacing of 2.53 Å of the nanowire. (c) A single wire was picked up by a probe using a nanorobotic manipulator installed inside an SEM. (d) The selected nanowire was fixed on the probe using FIB-CVD. (e) The setup for the electrical characterization of a single CuO NW.

The raw materials used for this experiment are as-grown CuO NWs. The synthesis of the nanowires begins with a copper foil [10]. After 2-hour incubation in a box oven at 500°C (Fig. 1(a)), the non-flaking nanowire arrays were grown on the surface of the copper substrate. The diameters of the nanowires ranged from 30 to 50 nm. The inset I of Fig. 1(a) shows an enlarged scanning electron microscope (SEM) image of a single nanowire. The inset II of Fig. 1(a) also shows that as-fabricated nanowires are distributed in the substrate at a high density of about 4~6 wires per 100 square nanometers. Furthermore, the high resolution TEM (HRTEM) image (Fig. 1(b)) indicates an inter-planar spacing of 2.53 Å, which demonstrates the excellent crystalline of the as-synthesized CuO NWs [11]. A single wire was attached on a probe using a nanorobotic manipulator (Fig. 1(c)) installed inside an SEM and then it was fixed in place using focused-ion-beam chemical vapor deposition (FIB-CVD) (Fig. 1(d)). The probe with the nanowire attached acted as a sample holder and was transferred into the TEM for characterization. A scanning tunneling microscope (STM) holder installed inside the TEM served as a nanomanipulator for the investigation. The nanowire was connected to another probe driven by the nanomanipulator from the other end (Fig. 1(e)), and electrical properties of this individual nanowire were measured simultaneously. Due to the insulate nature of the CuO NW, the measurement of the as-grown nanowire justified an dielectric behavior, therefore, a *forming* process is required to actuate the raw nanowires into memristors and enable them with the characteristic memristive switching behaviors [2, 4-5].

## III. E-BEAM-BASED MEMRISTOR FORMING

A number of memristor *forming* processes have been developed by previous investigations [2, 4, 6, 12]. Among them, electroforming [2, 6] and physical forming processes [4, 12] were most commonly used. However, the electroforming processes are unsuitable for the nanowire-based memristor device since the heat will cause a hard breakdown in the center of the CuO NW due to its cylindrical structure. Likewise, the physical forming is always carried out for several hours of annealing in a furnace and the inert gas should be injected at the same time, which can hardly be carried out *in situ*. For these reasons, we developed an e-beam-based *forming* method for the cylinder shaped memristors. By focusing the TEM electron beam on a part of the CuO NW, high energy electrons bombard the nanowire and expel oxygen atoms from the irradiated area in oxide materials [13]. Therefore, the CuO NW will be "de-oxidized". The forming process (Fig. 2(a)) shows that the e-beam is irradiating the nanowire that is fixed between the electrodes using the nanomanipulator. The irradiation current density was adjusted by changing the focus, the magnification, the brightness and the incident area. The empirical procedure of the forming process is: irradiates at a current density of 20 A/cm$^2$ on an area of $1.3\times10^{-14}$ cm$^2$ for 200 s. The accelerating voltage of the electron beam was kept at 200 kV in all experiments. The completion of the *forming*, which actuates CuO NW to the memristive device, can be identified *in situ* by electrical measurement or microscopy analysis. Since the dynamic resistance is the key character of memristive devices, the hysteresis *I-V* curve (Fig. 2(a)) symbolizes the *forming* of a memristor device. The HRTEM image (Fig. 2(b)) demonstrates the gradual forming process of the CuO NW with a distinct difference between the metalized segment and the pristine part. The irradiated area tends to become amorphous and can be easily seen from the image.

By analyzing the hysteresis *I-V* curve in Fig. 2(a), it can be noted that there are two distinctive reversible "off" and

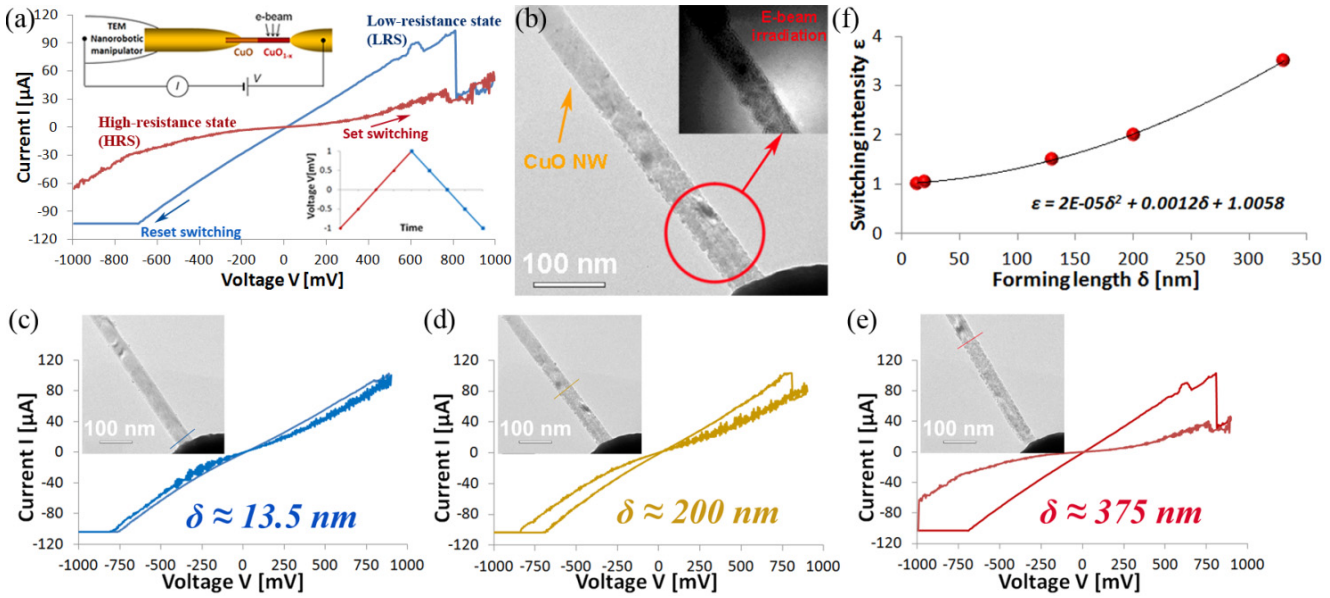


Fig.2 E-beam-based forming (a) The schematic of the e-beam-based and the insulator behavior of the original CuO NW was changed to memristive switching character during forming process. (b) The gradual forming process of the CuO NW demonstrated by using TEM. (c)(d)(e) The switching intensity is increased according to the increasing of forming area. (f) The relation between the switching intensity $\varepsilon$ and the forming length $\delta$ is: $\varepsilon = 0.0008\,\delta^2 + 0.0082\,\delta + 1.0036$.

"on" states in the memristor device. The off state corresponds to the high-resistance state (HRS) and the on state corresponds to the low-resistance state (LRS), and their resistances are defined as $R_{off}$ and $R_{on}$, respectively. As the applied voltage increases from 0 to the threshold voltage $V_{th} \approx 800mV$, the device switches from the off state to the on state, known as a "set" process. After decreasing the voltage and then reversing the direction to the reverse threshold voltage, the device went through a "reset" process change from on to off state. At any given voltages, the resistance can be either $R_{off}$ or $R_{on}$, depending on whether in memory of the previous applied positive or negative threshold voltage. Furthermore, we can define the magnitude of the switching by $\varepsilon$, the maximum value of $R_{off}/R_{on}$ in a hysteresis dual-curve. For various length $\delta$ of the irradiated area, the dynamic *I-V* characteristics are represented as a function of $\varepsilon$ (Fig. 2(c) to (e)). It is noted that a small area (e.g. $\phi$13.5 nm) of irradiation will be sufficient to induce visible memristive switching behavior. On the other hand, such behaviors may only be visible if the device is at nanometer scale. A larger irradiation area for forming the memristor will have potentially a larger $\varepsilon$, i.e., a higher switching intensity. Unexpectedly, the threshold voltage $V_{th}$ remains the same. This dynamic process provides an insight into the switching mechanism of CuO NW-based memristive devices.

## IV. Mechanism for CuO NW-based Memristors

There are several theories explaining the mechanism of memristors [1, 12]. It is believed that the CuO NW memristor is functionalized due to the conduction through oxygen dopants. To verify this, it is critical to justify the oxygen vacancy presence and migration *in situ*. Previous investigations on oxygen vacancies are mainly concentrated on detecting the structural or direct stoichiometry changes [14-15]. Instead of that, in this work we choose to detect the presense of $Cu^{1+}$ (transit from $Cu^{2+}$), which is a direct result of the existence of oxygen vacancies. Electron energy loss spectroscopy (EELS) is a multi-functional spectroscopy for measuring atomic composition, chemical bonding, surface properties, conduction band electronic properties and especially the change of valence state [16]. Since such methods can readily distinguish $Cu^{2+}$ and $Cu^{1+}$ and it is more sensitive to low concentration of oxygen vacancies and less depend on sample crystalinity due to damage by electron irradiation [17], the physical/chemical property changes that are responsible for the memristive switching can be studied *in situ* using EELS technique.

Cu $L_{2,3}$ edge spectra (Fig. 3(a)) at two distinctive areas on the nanowire with the pristine unirradiated portion (CuO) and the irradiated portion ($CuO_{1-x}$). The standard $Cu^{2+}$ and $Cu^{1+}$ spectra superimposed is inserted as references, showing the distinctive difference between the $L_3/L_2$ peak intensity ratio for $Cu^{2+}$ and $Cu^{1+}$. The spectrum before the irradiation coincides with $Cu^{2+}$ very well, proving its 100% CuO composition, while the spectrum after the irradiated lies in between that of $Cu^{2+}$ and $Cu^{1+}$. Therefore, the irradiated part can be represented by $CuO_{1-x}$ which is a mixture of $Cu_2O$ and CuO. The creation of $Cu^{1+}$ after the irradiation proves the loss of oxygen, i.e., creation of oxygen vacancies. The amount of oxygen vacancies is qualitatively represented by the excessive $L_2$ peak intensity relative to that of $Cu^{2+}$. Cu $L_{2,3}$ edge at the unirradiated CuO area (point A) before and after the memristor setting process, i.e., an applied voltage greater than $V_{th}$. It is clear that the spectrum after the switching voltage has a higher $L_2$ peak intensity than that before, indicating the presence of oxygen vacancies. Since

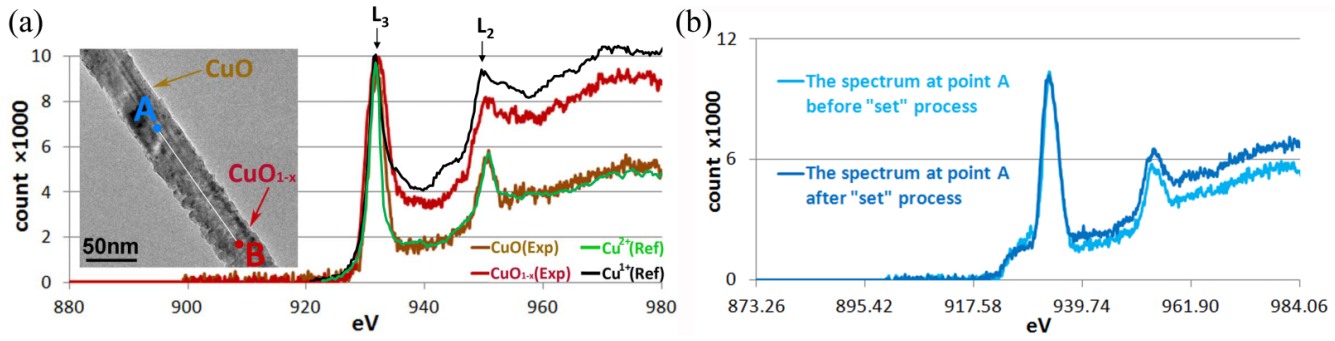


Fig.3 The characterization of the deoxidized segment. The Cu $L_{2,3}$ edge spectra of the pristine nanowire and the segment after the electron irradiation, with standard $Cu^{2+}$ and $Cu^{1+}$ spectra superimposed as references. The pristine segment is coincided with $Cu^{2+}$ very well, proving its 100% CuO composition. The segment after the e-beam irradiation shows an intermediate state between the $Cu^{2+}$ and the $Cu^{1+}$. We termed the state as $CuO_{1-x}$ (a mixture of $Cu_2O$ and CuO).

there is no loss of overall oxygen atoms by applying a voltage, the oxygen vacancies can only be migrated from $CuO_{1-x}$ area.

Now a complete mechanism for CuO NW-based memristors can be illustrated schematically (Fig. 4). The initial forming process de-oxidizes CuO thus creates abundant oxygen vacancies, represented by small circles (Fig. 4(a)). However, these localized oxygen vacancies do not conduct through the nanowire, so the nanowire will stay at a high resistivity off state. The oxygen vacancies are forced to migrate under an external bias and eventually channeling through the nanowire when the voltage reaches the threshold $V_{th}$ (Fig. 4(b)). Then, the oxygen vacancies become the major charge carriers such that the nanowire switches to a low resistivity on state. Oxygen vacancies will remain as the charge carriers thus "remember" its low resistivity state. Only when a high reverse resetting threshold voltage is applied, the oxygen vacancies are forced to reversely migrate and eventually disconnect the conduction path (Fig. 4(c)). Then the nanowire device returns to its high resistivity off state. Again, with a bias lower than the setting voltage applied, it will remember its high resistivity state.

As we carried out the EELS measurement in a scanning transmission electron microscope (STEM), the EEL spectra along the nanowire can be continuously measured. A scanning oxygen EEL spectrum topology along the nanowire can be plotted, and the oxygen distributions *in situ* before and after the set process or reset process can be documented. Then, by comparing these spectrum topologies, the migration trend of the oxygen vacancies can be measured, which in turn provides a solid evidence for the migration-based switching. The STEM-EELS technique was carried out across the nanowire from point A to point B (Fig. 4(a)). The continuous Cu $L_{2,3}$ edge EELS profile as plotted (Fig. 4(d) to (f)) are corresponding to each state in Fig. 4(a) to (c), respectively. Fig. 4(d) represents the spectra profile from point A to B at the initial state after forming, corresponding to Fig. 4(a). In order to give a clear visual effect, we deliberately set the color scheme so that the red color is directly correlated to the excessive $L_2$ peak intensity above that of $Cu^{2+}$. Therefore, the fact that there is no red signal at point A area further indicates that there are no oxygen vacancies. The excessive intensity of $L_2$ at point B area is represented as red color, representing the oxygen vacancy qualitatively. Moreover, the spectrums at points A and B were also plotted (Fig. 4(a)). It is noted that there is a large gap between these two spectrums, indicating the oxygen vacancies density difference at these two points. However, the gap between these two spectrums was narrowed after the set switching process (Fig. 4(b)), which implies that the oxygen vacancies have changed at these two points. Furthermore, it is noted that there is clearly a red signal appears at $L_2$ peak for point A area from the spectra profile (Fig. 4(e)), accompanied by a slightly reduced red signal at area B. This is a direct evidence of the migration of the oxygen vacancies from B to A. After the reset switching process, the spectra profile (Fig. 4(f)) shows the disappearing of the red signal at $L_2$ peak in area A and the gap between the spectra in A and B (Fig. 4(b)) was opened again, indicating the reversal of oxygen vacancy migration.

## V. Memsensor

In addition to the commonly anticipated NVRAM applications using memristors, we explore the possibility for "memsensors" based on nanowire memristor that has a "memory" of other physical quantities, such as mechanical deformation/force.

The characteristic *I-V* curves at various deformations applied to the CuO NW are demonstrated (Fig. 5). By measuring the variation of set switching bias during the stressing, the nanowire displacement can be achieved, forming a displacement transducer. The switching threshold voltage $V_{th}$ was decreased from 280 mV to 155 mV when the nanowire was deformed (Fig. 5(a)). The nanowire is bending as the attached probe is moved back and forth. We define the deformation ratio as σ, which represents the ratio of the chord length between the deformed the nanowire and the original one. The displacement of the attached probe is measured by the deformation of the bending wire accordingly. Thus, the relations between the deformation ratio and the $V_{th}$ (Fig. 5(b)) can be expressed as: $V_{th} = -2.6057\sigma + 289.42$.

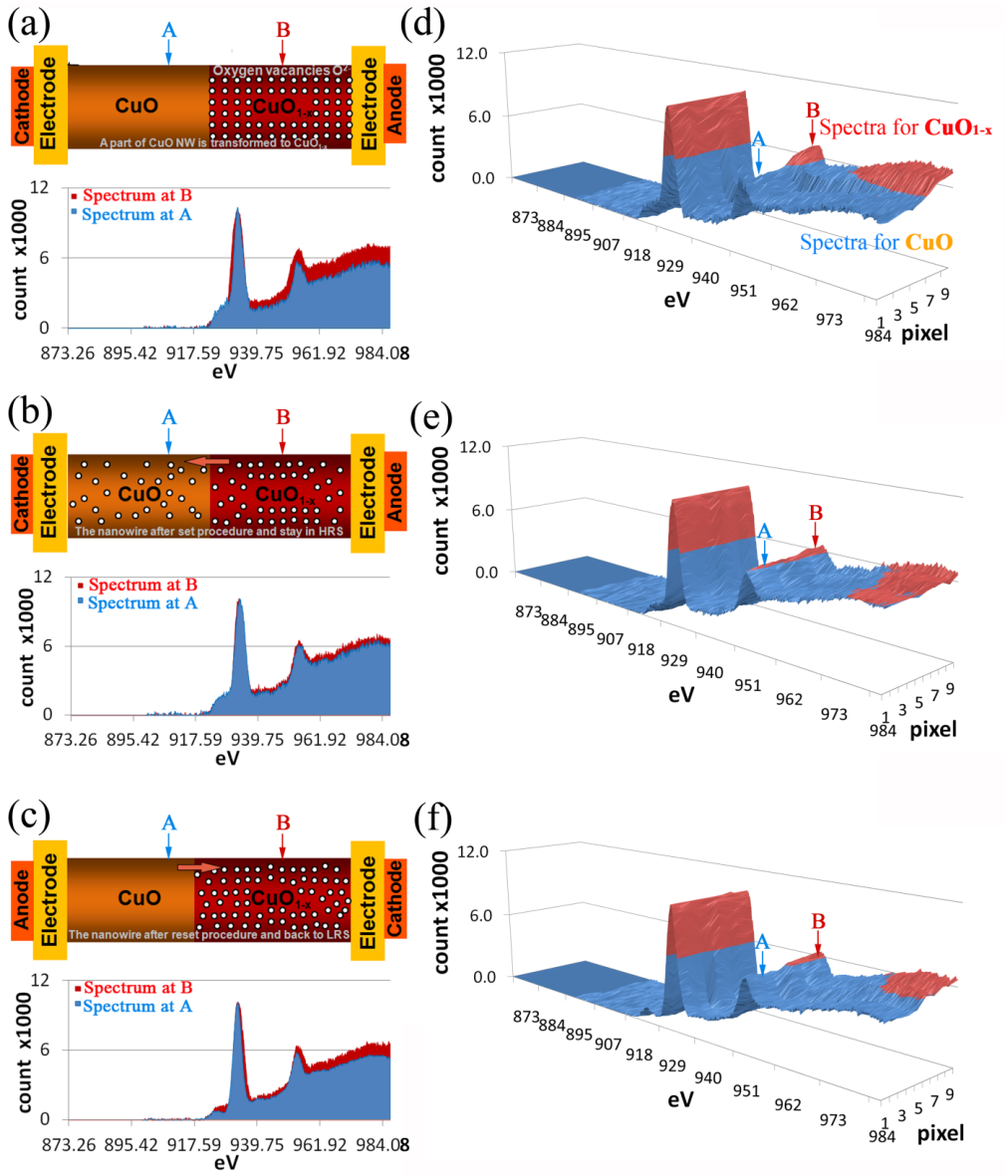


Fig.4 The proof of the migration of oxygen vacancies. (a) The model of the nanowire that after the forming process. After the forming of a part of CuO NW to $CuO_{1-x}$, the oxygen cations are excessive in this segment due to the loss of oxygen atoms. The spectrum at B shows an oxygen vacancies rich performance when it compared with the spectrum at point A. (b) The model of the nanowire after the set procedure (from HRS to LRS). Set procedure: the anode is placed on the part of $CuO_{1-x}$ and the cathode is in the CuO side. As sweeping the bias between two electrodes, the vacancies in $CuO_{1-x}$ part are transport all through the nanowire that drives by the electric force. Meanwhile, the electrons pass through the conductive paths that explored by the cations. Therefore, the conductivity decreased. The gap between the spectrum at point A and point B is narrowed, which indicates the migration of oxygen vacancies from B to A. (c) The model of the nanowire after the reset procedure (from LRS to HRS). To switch from LRS to HRS (reset procedure), the electric force direction was switched according to the alternate of external polar, which in turn broke the conductive path along the nanowire and makes the resistance back to the original high status. The gap between the two spectra opened again, which indicates the reversal migration of the oxygen vacancies from A to B. (d) The STEM-EEL spectra of the CuO NW after the forming process. The spectra topology represents the distinguish oxygen vacancy density difference along the nanowire. (e) The STEM-EEL spectra of the CuO NW after the set procedure. The spectra topology clearly indicates the migration of the oxygen vacancies from rich area (B) to the poor area (A). (f) The correspondent STEM-EEL spectra for the CuO NW after the reset switching process. The reversal of $O^{2-}$ migration is clearly indicated.

This result strongly implies that we may have achieved a new device as we defined as “memsensor”. For instance, without an external stress, when the voltage was kept at a constant intermediate value, e.g. 200 mV, the nanowire should keep its resistance since it is below the threshold voltage. By applying an external stress, it is possible to lower the memristor switching threshold voltage $V_{th}$ below 200 mV, thus the memristor will have a transition from high resistance state to low resistance state. Also, it will remain at the low resistance state even if the stress is withdrawn. In other words, this memristor will have memory of external stress instead of external voltage. It demonstrated the principle of memsensor which can be achieved by combining memristor properties with other sensory

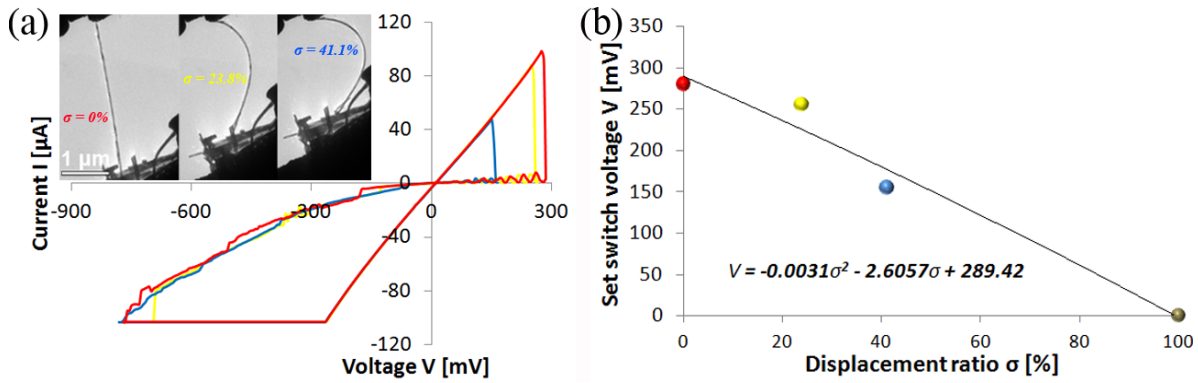


Fig.5 The application of CuO NW-based memristor as a displacement transducer. (a) The switching threshold voltage $V_{th}$ was decreased according to the increasing of the deformation ratio σ. The displacement of the attached probe is measured by the deformation of the bending wire. (b) The relations between the switching threshold voltage $V_{th}$ and the displacement ratio σ can be read out as: $V_{th} = -2.6057\sigma + 289.42$.

properties. While the detailed mechanism of CuO under a stress is not fully understood yet, one of the interpretations is that CuO NW may have a piezoelectric property which generates extra voltage under a stress.

## VI. Conclusions

In summary, we have developed a memristor nanodevice based on an individual CuO NW. The forming process depends on irradiation-beam-induced local de-oxidization of a segment of a CuO NW. The memristivity of this device is characterized by dynamic hysteretic current-voltage curves. By using the EELS technique to investigate the switching mechanism, we have not only confirmed the creation of oxygen vacancies in CuO NWs at the forming process, but also *in situ* quantified the migration of the oxygen vacancies, which is responsible for the memristive switching in our memristor device. The nanowire-based memristor has the potential to be combined with other sensing elements to form new types of memsensor devices. One such memsensor has been demonstrated with a combination with mechanical displacement sensor. Therefore nanowire-based memristor shows great potential for designing all kinds of low-power high-throughput memory units and other functional nanodevices.

## Acknowledgement

This work is partially supported by the NSF (IIS-1054585)

## References

[1] D. B. Strukov, G. S. Snider, D. R. Stewart, and R. S. Williams, "The missing memristor found," *Nature,* vol. 453, no. 7191, pp. 80-83, May 2008.

[2] D. S. Jeong, H. Schroeder, U. Breuer, and R. Waser, "Characteristic electroforming behavior in Pt/$TiO_2$/Pt resistive switching cells depending on atmosphere," *Journal of Applied Physics,* vol. 104, no. 12, art. no. 123716, Dec 2008.

[3] B. J. Choi, D. S. Jeong, S. K. Kim, C. Rohde, S. Choi, J. H. Oh, H. J. Kim, C. S. Hwang, K. Szot, R. Waser, B. Reichenberg, and S. Tiedke, "Resistive switching mechanism of $TiO_2$ thin films grown by atomic-layer deposition," *Journal of Applied Physics,* vol. 98, no. 3, art. no. 033715, Aug 2005.

[4] J. J. Yang, M. D. Pickett, X. M. Li, D. A. A. Ohlberg, D. R. Stewart, and R. S. Williams, "Memristive switching mechanism for metal/oxide/metal nanodevices," *Nature Nanotechnology,* vol. 3, no. 7, pp. 429-433, Jul 2008.

[5] D.-H. Kwon, K. M. Kim, J. H. Jang, J. M. Jeon, M. H. Lee, G. H. Kim, X.-S. Li, G.-S. Park, B. Lee, S. Han, M. Kim, and C. S. Hwang, "Atomic structure of conducting nanofilaments in $TiO_2$ resistive switching memory," *Nature Nanotechnology,* vol. 5, no. 2, pp. 148-153, Feb 2010.

[6] R. Waser and M. Aono, "Nanoionics-based resistive switching memories," *Nature Materials,* vol. 6, no. 11, pp. 833-840, Nov 2007.

[7] W. Z. Wu and Z. L. Wang, "Piezotronic Nanowire-Based Resistive Switches As Programmable Electromechanical Memories," *Nano Letters,* vol. 11, no. 7, pp. 2779-2785, Jul 2011.

[8] Q. Liu, J. Sun, H. B. Lv, S. B. Long, K. B. Yin, N. Wan, Y. T. Li, L. T. Sun, and M. Liu, "Real-Time observation on dynamic growth/dissolution of conductive filaments in oxide-electrolyte-based ReRAM," *Advanced Materials,* vol. 24, no. 14, pp. 1844-1849, Apr 2012.

[9] Y. C. Yang, P. Gao, S. Gaba, T. Chang, X. Q. Pan, and W. Lu, "Observation of conducting filament growth in nanoscale resistive memories," *Nature Communications,* vol. 3, art. no. 732, Mar 2012.

[10] F. Mumm and P. Sikorski, "Oxidative fabrication of patterned, large, non-flaking CuO nanowire arrays," *Nanotechnology,* vol. 22, no. 10, art. no. 105605, Mar 2011.

[11] X. C. Jiang, T. Herricks, and Y. N. Xia, "CuO nanowires can be synthesized by heating copper substrates in air," *Nano Letters,* vol. 2, no. 12, pp. 1333-1338, Dec 2002.

[12] D. S. Jeong, H. Schroeder, and R. Waser, "Coexistence of bipolar and unipolar resistive switching behaviors in a Pt/$TiO_2$/Pt stack," *Electrochemical and Solid State Letters,* vol. 10, no. 8, pp. 51-53, Mar 2007.

[13] L. A. Bursill and A. C. McLaren, "Transmission electron microscope study of natural radiation damage in zircon ($ZrSiO_4$)," *Physica Status Solidi,* vol. 13, no. 2, pp. 331-343, 1966.

[14] Z. L. Liao, P. Gao, X. D. Bai, D. M. Chen, and J. D. Zhang, "Evidence for electric-field-driven migration and diffusion of oxygen vacancies in Pr0.7Ca0.3MnO3," *Journal of Applied Physics,* vol. 111, no. 11, art. no. 114506, Jun 2012.

[15] Y. M. Kim, J. He, M. D. Biegalski, H. Ambaye, V. Lauter, H. M. Christen, S. T. Pantelides, S. J. Pennycook, S. V. Kalinin, and A. Y. Borisevich, "Probing oxygen vacancy concentration and homogeneity in solid-oxide fuel-cell cathode materials on the subunit-cell level," *Nature Materials,* vol. 11, no. 10, pp. 888-894, Oct 2012.

[16] R. F. Egerton, *Electron energy-loss spectroscopy in the electron microscope*, 3rd ed. New York: Springer, 2011.

[17] R. D. Leapman, L. A. Grunes, and P. L. Fejes, "Study of the $L_{23}$ Edges in the *3d* transition-metals and their oxides by electron-energy-loss-spectroscopy with comparisons to theory," *Physical Review B,* vol. 26, no. 2, pp. 614-635, 1982.